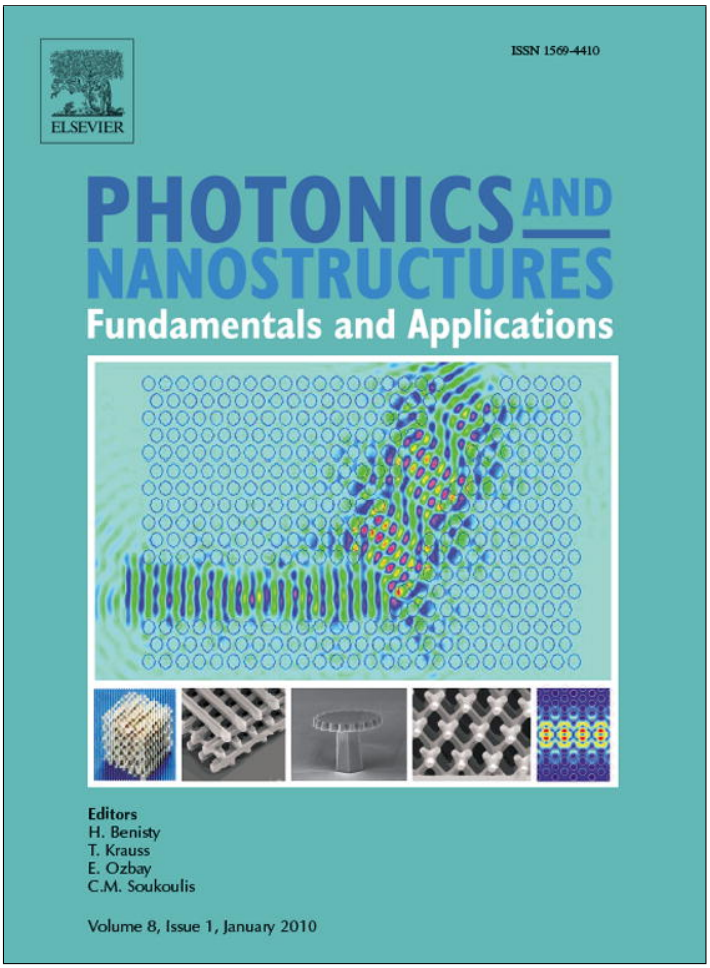

Available online at www.sciencedirect.com
ScienceDirect
Photonics and Nanostructures – Fundamentals and Applications 8 (2010) 23–31
PHOTONICS AND NANOSTRUCTURES Fundamentals and Applications
www.elsevier.com/locate/photonics

Dynamical Green's function theory to study the optical phenomena related to metamaterials

Weihua Wang, Xueqin Huang, Lei Zhou *

Surface Physics Laboratory (State Key Laboratory) and Physics Department, Fudan University, Shanghai 200433, PR China

Received 12 August 2009; accepted 18 January 2010
Available online 25 January 2010

Abstract

We combine a space–time Lorentz transformation with a dyadic Green's function technique to establish a general and rigorous dynamical theory, which can be employed to study the optical phenomena occurring in a moving environment. As the applications of this method, we studied the Doppler effects of a source moving near a metamaterial slab and the super imaging effect achieved by a moving metamaterial lens. Many interesting anomalous phenomena were discovered, induced typically by the interplays between the source and the surface waves of the metamaterial slab.

Keywords: Metamaterials; Doppler effect; Super lensing; Green's function; Surface wave

1. Introduction

Metamaterials, artificial electromagnetic (EM) materials constituted by subwavelength local resonant structures, have attracted intensive attention recently [1–3]. Engineered by the microstructures which can provide electric and/or magnetic resonances, the entire medium can exhibit arbitrary values of effective permittivity ε and permeability μ. In particular, when both ε and μ are negative, the medium exhibits a negative refractive index [1–4], so that it is sometimes termed as a left-handed material [1–4]. Many unusual optical effects, which are typically unrealizable with conventional materials, were proposed or realized based on metamaterials. These include the negative refraction [1–5], super lensing effect [5–7], inverse Doppler and Cerenkov effects [8–14], extraordinary photonic band gap effects [15,16], and even the invisible cloaking [17,18], etc.

In reviewing these previous studies, we found that while there were quite a lot of efforts in studying the metamaterial-related optical effects generated by a *static* radiating source [5–7,15–18], the theoretical developments are still not satisfactory for the situations where the sources and medium are in relative motions. For instance, to study the Doppler effects, some previous theoretical studies employed a *Galileo* transformation to treat the movements of the source and receiver, and considered a plane wave source which is not so realistic [8–14]. On the other hand, it is also interesting to ask how those intriguing phenomena, such as the super lensing [5–7] and the invisible cloaking effects [17,18], evolve when the source is in relative motion with respect to the medium. Such problems are highly nontrivial since the metamaterials must be frequency dispersive due to the causality requirement [19], and therefore, their responses to a moving source could be rather intriguing and may generate many unexpected new phenomena.

* Corresponding author.
E-mail address: phzhou@fudan.edu.cn (L. Zhou).

1569-4410/$ – see front matter
doi:10.1016/j.photonics.2010.01.001

The motivation of this paper is to set up a general and rigorous theoretical framework to study the metamaterial-related optical effects in the cases when the source, receiver, and the medium are in relative motions. We will combine the *Lorentz* space–time transformation [20,21] with the time-dependent dyadic Green's function method [21,22] to achieve this goal. We have already employed a special form of the general approach to study the Doppler effects of a light source moving on the surface of a dispersive metamaterial slab [23]. Here, we present all the details of mathematic derivations of the general theory, and employ the theory to study some other intriguing optical effects related to moving source/medium.

The present paper is organized as follows. We first establish the theoretical framework in the next section, and present some benchmark results in Section 3. We then apply the theory to study the anomalous Doppler effects and the super lensing effect in Section 4. We finally conclude our paper in Section 5.

2. The dynamical theory for moving source/medium

We take a particular situation as an example to establish the theoretical framework, and the theory can be generalized to more complicated situations. As shown in Fig. 1, we consider the cases that the source and receiver are moving at different velocities, $\hat{v}_s = v_s(\cos\theta_s\hat{e}_x + \sin\theta_s\hat{e}_z)$, $\hat{v}_r = v_r(\cos\theta_r\hat{e}_x + \sin\theta_r\hat{e}_z)$, with respect to a metamaterial slab placed on the xy plane lying between $z = -0.5d$ and $z = -1.5d$ (We set $d = 10$ mm in all our calculations). We assume that the permittivity and permeability of the metamaterial slab are given by $\varepsilon_r(\omega)$, $\mu_r(\omega)$. Since both the source and receiver are moving, we define three frames—S' frame where the source is static, S frame where the slab is static and $\tilde{S}$ frame where the receiver is static. As usual, we assume that the origins of these three frames coincide at $t' = t = \tilde{t} = 0$. For simplicity, our source is assumed as a line current source taking the following

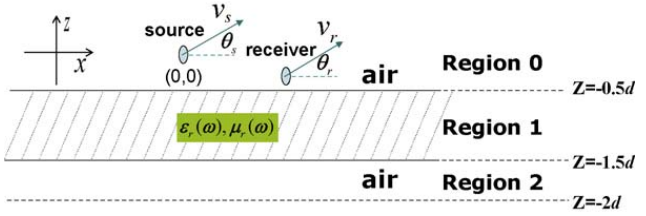

Fig. 1. Schematic shown of the studied geometry.

form

$$\vec{J}'(\vec{r}', t') = \hat{e}_y I_0 \delta(x')\delta(z')e^{-i\omega_0 t'}\theta(t'). \tag{1}$$

The source is located at the origin in the S' frame (See Fig. 1) and start to emit EM signals at $t' = 0$ [Noting that there is a $\theta(t')$ function in Eq. (1)]. Apparently, there is no charge accumulation in the line source, i.e., $\rho'(\vec{r}', t') = 0$. Our goal is to find the field distribution in the $\tilde{S}$ frame so that we can get the signal measured by the receiver. We will achieve this goal following three steps:

(1) We first calculate the EM fields radiated from the source in the S' frame, assuming at the moment that there is no metamaterial slab;
(2) we next employ a Lorentz transformation to transform such EM fields from the S' frame to S frame, then "put" the metamaterial slab into the frame and calculate the scatterings of these EM waves by the metamaterial slab;
(3) we finally apply another Lorentz transformation to obtain the entire field distributions in the $\tilde{S}$ frame.

2.1. Incident EM waves observed in the S' frame

In this subsection, let us "remove" the metamaterial slab for a moment. In the S' frame where the source is static, EM waves satisfy

$$\begin{cases} \left[\nabla\times\nabla\times + \mu_0\varepsilon_0\dfrac{\partial^2}{\partial t'^2}\right]\vec{E}'(\vec{r}', t') = -\mu\dot{\vec{J}}'(\vec{r}', t') \\ \left[\nabla\times\nabla\times + \mu_0\varepsilon_0\dfrac{\partial^2}{\partial t'^2}\right]\vec{H}'(\vec{r}', t') = \nabla\times\vec{J}'(\vec{r}', t') \end{cases} \tag{2}$$

Define a dyadic Green's function by

$$\left(\nabla\times\nabla\times + \mu_0\varepsilon_0\frac{\partial^2}{\partial t'^2}\right)\vec{\vec{G}}(\vec{r}', \vec{r}_1'; t', t_1') = \delta(\vec{r}' - \vec{r}_1')\delta(t' - t_1')\vec{\vec{I}}, \tag{3}$$

we found that

$$\begin{cases} \vec{E}'(\vec{r}', t') = -\mu_0\displaystyle\int \vec{\vec{G}}(\vec{r}', \vec{r}_1'; t', t_1')\cdot\dot{\vec{J}}'(\vec{r}', t')d\vec{r}_1'dt_1' \\ \vec{H}'(\vec{r}', t') = \displaystyle\int \vec{\vec{G}}(\vec{r}', \vec{r}_1'; t', t_1')\cdot\left[\nabla\times\vec{J}'(\vec{r}', t')\right]d\vec{r}_1'dt_1' \end{cases}, \tag{4}$$

where the Green's function [21,22] is given by

$$\begin{aligned}\overrightarrow{\overrightarrow{G}}(\vec{r}',\vec{r}_1';t',t_1') &= \frac{1}{(2\pi)^4}\iiint dk_x dk_y dk_z d\omega e^{-i\omega(t'-t_1')}e^{i\vec{k}\cdot\left(\vec{r}'-\vec{r}_1'\right)} \\ &\times \frac{1}{k_x^2+k_y^2+k_z^2-k^2}\left[\bar{\bar{I}}-\frac{\vec{k}\vec{k}}{k^2}\right]. \end{aligned} \tag{5}$$

Therefore, the EM waves radiated from the source seen at the S' frame can be easily obtained by putting Eqs. (1) and (5) into Eq. (4) and performing the integrations. For example, the y-component of electric field is found as

$$E_y'(\vec{r}',t') = \frac{i\mu_0 I_0}{8\pi^2}\int dk_x' d\omega' e^{-i\omega' t'}e^{ik_x' x'}e^{ik_{0z}'|z'|}\frac{1}{k_{0z}'} \times \frac{\omega'}{\omega'-\omega_0+i\eta}, \tag{6}$$

where

$$k_{0z}' = \sqrt{(\omega'/c)^2 - k_x'^2} \geq 0. \tag{7}$$

Here $\omega', \vec{k}'$ are the frequency and wavevector of the EM wave in the S' frame; c is the speed of light in vacuum, and η is a very small constant to ensure the causality (we set $\eta = 10^{-4}$ GHz in all numerical calculations). It is worth noting that the field expressions are different for $z' > 0$ and $z' < 0$ [see Eq. (6)], since there is a source located at $z' = 0$. To avoid making the mathematics too complicated, we assume in this paper that the metamaterial slab and the receiver are *always* lying in the $z' < 0$ region, which require that $\sin\theta_s > 0$ and $v_s \sin\theta_s \geq v_r \sin\theta_r$. While the extensions to general situations are doable in principle, the resulting field expressions are too cumbersome, making it difficult to understand the simple physics. Under this condition, we only need to consider the $z' < 0$ branch in Eq. (6) in all our calculations followed, which simplifies the mathematics significantly.

2.2. Field distributions in the S frame

We now apply a space–time transformation to calculate such EM fields observed in the S frame. According to the special theory of relativity, the EM fields in two different frames are related by [21],

$$\begin{bmatrix}\vec{E}\\ c\vec{B}\end{bmatrix} = \gamma\begin{bmatrix}\bar{\bar{\alpha}}^{-1} & \bar{\bar{\beta}}\\ -\bar{\bar{\beta}} & \bar{\bar{\alpha}}^{-1}\end{bmatrix}\cdot\begin{bmatrix}\vec{E}'\\ c\vec{B}'\end{bmatrix}. \tag{8}$$

where

$$\bar{\bar{\beta}} = \begin{bmatrix}0 & \beta_s\sin(\theta_s) & 0\\ -\beta_s\sin(\theta_s) & 0 & \beta_s\cos(\theta_s)\\ 0 & -\beta_s\cos(\theta_s) & 0\end{bmatrix}$$

$$\bar{\bar{\alpha}}^{-1} = \begin{bmatrix}\sin^2(\theta_s)+\dfrac{\cos^2(\theta_s)}{\gamma_s} & 0 & (\gamma_s-1)\cos(\theta_s)\sin(\theta_s)\\ 0 & 1 & 0\\ (\gamma_s-1)\cos(\theta_s)\sin(\theta_s) & 0 & \cos^2(\theta_s)+\dfrac{\sin^2(\theta_s)}{\gamma_s}\end{bmatrix}, \tag{9}$$

are the Lorentz transformation matrixes linking S' and S frames with $\beta_s = v_s/c$, $\gamma_s = (1-\beta_s^2)^{-1/2}$. Employing a further Lorentz transformation to change the coordinates $\{\vec{r}',t'\}$ to $\{\vec{r},t\}$, we finally got all the fields $\{\vec{E}(\vec{r},t),\vec{B}(\vec{r},t)\}$ in the S frame (assuming that there is still no metamaterial slab at this moment). For example, we find that

$$E_y(\vec{r},t) = \frac{i\mu_0 I_0}{8\pi^2}\int dk_x d\omega e^{-i\omega t}\Omega(\omega,k_x)e^{ik_x x}e^{-ik_{0z}z}, \tag{10}$$

where $\left(\vec{k},\omega\right)$ are the wavevector and frequency defined in S frame and are related to $\left(\vec{k}',\omega'\right)$ by

$$\begin{cases}\omega' = \gamma_s\omega - \gamma_s\vec{\beta}_s\cdot c\vec{k}\\ \vec{k}' = \bar{\bar{\alpha}}\cdot\vec{k} - \gamma_s\vec{\beta}_s\dfrac{\omega}{c}\end{cases}, \tag{11}$$

and the function $\Omega(\omega,k_x)$ is defined as

$$\Omega(\omega,k_x) = \frac{\omega}{\left[1+(\gamma_s-1)\sin^2(\theta_s)\right]k_{0z} - (\gamma_s-1)\cos(\theta_s)\sin(\theta_s)k_x + \gamma_s\sin(\theta_s)\beta_s\,\omega/c} \times \frac{1}{\gamma_s[\omega-\cos(\theta_s)c\beta_s k_x + \sin(\theta_s)c\beta_s k_{0z}] - \omega_0 + i\eta}. \tag{12}$$

We note that Eq. (10) has clear physical interpretations—the EM wave radiated from a moving source (seen at the S frame) contains a series of plane waves characterized by ω and $\vec{k}$, with $\Omega(\omega,k_x)$ being the corresponding weighting coefficient. In the limiting case when the source is static (i.e., $v_s = 0$), we find from Eq. (12) that $\Omega(\omega,k_x) = \omega/[k_{0z}\cdot(\omega-\omega_0+i\eta)]$, recovering the static-source case as shown in Eq. (6).

We now "put" the metamaterial slab inside this frame. Since the wave incident on the metamaterial slab is already expressed as a sum of plane waves [Eq. (10)],

we can study the transmission/reflection problems by treating each plane wave component separately. According to the layered Green's function theory [21,22], we can get the entire EM field distributions in this frame straightforwardly. Still taking E_y as an example, we find its expression in region 0 (see Fig. 1) as

$$E_y(\vec{r},t) = \frac{i\mu_0 I_0}{8\pi^2}\int d\omega dk_x e^{-i\omega t}e^{ik_x x}\Omega(\omega,k_x) \times (e^{-ik_{0z}z} + R^{\mathrm{TE}}e^{ik_{0z}z}), \tag{13}$$

and its expression in region 2 (see Fig. 1) as

$$E_y(\vec{r},t) = \frac{i\mu_0 I_0}{8\pi^2}\int d\omega dk_x e^{-i\omega t}e^{ik_x x}\Omega(\omega,k_x)T^{\mathrm{TE}}e^{-ik_{0z}z}. \tag{14}$$

where R^{TE} and T^{TE} are the reflection and transmission coefficients for a particular plane wave characterized by ω and k_x. They are defined as

$$\begin{aligned} T^{\mathrm{TE}}(\omega,k_x) &= \frac{4\triangle e^{-ik_{0z}d}}{(\triangle+1)^2 e^{-ik_{1z}d} - (\triangle-1)^2 e^{ik_{1z}d}} \\ R^{\mathrm{TE}}(\omega,k_x) &= \frac{(1-\triangle^2)(1-e^{ik_{1z}2d})e^{ik_{0z}d}}{(\triangle+1)^2 - (\triangle-1)^2 e^{ik_{1z}2d}} \end{aligned}, \tag{15}$$

with

$$\triangle = \frac{k_{1z}\mu_0}{k_{0z}\mu_1} = \frac{\sqrt{\varepsilon_{\mathrm{r}}(\omega)\mu_{\mathrm{r}}(\omega)\,\omega^2/c^2 - k_x^2}}{k_{0z}\mu_{\mathrm{r}}(\omega)}. \tag{16}$$

We note that Eq. (13) is obtained under the assumption we only take the $z' < 0$ branch in Eq. (6).

2.3. Field distributions in the $\tilde{S}$ frame

We now calculate the field distributions in the $\tilde{S}$ frame, following the same procedures as we transform the fields from S' to S frames. The only difference here is that we need to separately treat the incident wave and the reflected wave, which behave differently when we transform the frames. After a tedious but straightforward calculation, we find all the fields in the $\tilde{S}$ frame. For example, the E_y component is found to take the following form in region 0

$$\tilde{E}_y(\tilde{\vec{r}},\tilde{t}) = \frac{i\mu_0 I_0}{8\pi^2}\int d\tilde{\omega}d\tilde{k}_x e^{-i\tilde{\omega}\tilde{t}}e^{i\tilde{k}_x\tilde{x}} \left[\Omega_-(\tilde{\omega},\tilde{k}_x)e^{-i\tilde{k}_{0z}\tilde{z}} + \Omega_+(\tilde{\omega},\tilde{k}_x)\tilde{R}^{\mathrm{TE}}e^{i\tilde{k}_{0z}\tilde{z}}\right], \tag{17}$$

and take the following form

$$\tilde{E}_y(\tilde{\vec{r}},\tilde{t}) = \frac{i\mu_0 I_0}{8\pi^2}\int d\tilde{\omega}d\tilde{k}_x e^{-i\tilde{\omega}\tilde{t}}e^{i\tilde{k}_x\tilde{x}}\Omega_-(\tilde{\omega},\tilde{k}_x)\tilde{T}^{\mathrm{TE}}e^{-i\tilde{k}_{0z}\tilde{z}}. \tag{18}$$

in region 2. We note that Eqs. (17) and (18) are similar to Eqs. (13) and (14) except the spectra functions $\Omega_\pm$, which are now different for waves travelling along two directions. The spectra functions $\Omega_\pm$ are defined as

$$\Omega_\mp(\tilde{\omega},\tilde{k}_x) = \frac{1}{C_\mp\tilde{k}_{0z} + D_\mp\tilde{k}_x + E_\mp\,\tilde{\omega}/c} \frac{\tilde{\omega}}{L_\mp\tilde{k}_{0z} + M_\mp\tilde{k}_x + N_\mp\tilde{\omega} - \omega_0 + i\eta}. \tag{19}$$

$$\left\{\begin{aligned} C_\mp &= \left[\cos^2\theta_{\mathrm{s}} + \gamma_{\mathrm{s}}\sin^2\theta_{\mathrm{s}}\right]\left[\cos^2\theta_{\mathrm{r}} + \gamma_{\mathrm{r}}\sin^2\theta_{\mathrm{r}}\right] \pm (\gamma_{\mathrm{s}}-1)(\gamma_{\mathrm{r}}-1)\frac{\sin(2\theta_{\mathrm{s}})\sin(2\theta_{\mathrm{r}})}{4} \\ &\quad \mp \gamma_{\mathrm{s}}\gamma_{\mathrm{r}}\beta_{\mathrm{s}}\beta_{\mathrm{r}}\sin(\theta_{\mathrm{s}})\sin(\theta_{\mathrm{r}}) \\ D_\mp &= \gamma_{\mathrm{s}}\gamma_{\mathrm{r}}\beta_{\mathrm{s}}\beta_{\mathrm{r}}\sin(\theta_{\mathrm{s}})\cos(\theta_{\mathrm{r}}) \mp (\gamma_{\mathrm{r}}-1)\frac{\sin(2\theta_{\mathrm{r}})}{2}\left[\cos^2(\theta_{\mathrm{s}}) + \gamma_{\mathrm{s}}\sin^2(\theta_{\mathrm{s}})\right] \\ &\quad -(\gamma_{\mathrm{s}}-1)\frac{\sin(2\theta_{\mathrm{s}})}{2}\left[\cos^2(\theta_{\mathrm{r}}) + \gamma_{\mathrm{r}}\sin^2(\theta_{\mathrm{r}})\right] \\ E_\mp &= \gamma_{\mathrm{s}}\gamma_{\mathrm{r}}\beta_{\mathrm{s}}\sin(\theta_{\mathrm{s}}) \mp \gamma_{\mathrm{r}}\beta_{\mathrm{r}}\sin(\theta_{\mathrm{s}})\left[\cos^2(\theta_{\mathrm{s}}) + \gamma_{\mathrm{s}}\sin^2(\theta_{\mathrm{s}})\right] \\ &\quad -(\gamma_s-1)\gamma_{\mathrm{r}}\beta_{\mathrm{r}}\frac{\sin(2\theta_{\mathrm{s}})\cos(\theta_{\mathrm{r}})}{2} \\ L_\mp &= \gamma_{\mathrm{s}}\sin(\theta_{\mathrm{s}})c\beta_{\mathrm{s}}\left[\cos^2(\theta_{\mathrm{r}}) + \gamma_{\mathrm{r}}\sin^2(\theta_{\mathrm{r}})\right] \\ &\quad \pm\gamma_{\mathrm{s}}(\gamma_{\mathrm{r}}-1)c\beta_{\mathrm{s}}\cos(\theta_{\mathrm{s}})\frac{\sin(2\theta_{\mathrm{r}})}{2} \mp \gamma_{\mathrm{s}}\gamma_{\mathrm{r}}c\beta_{\mathrm{r}}\sin(\theta_{\mathrm{r}}) \\ M_\mp &= \gamma_{\mathrm{s}}\gamma_{\mathrm{r}}c\beta_{\mathrm{r}}\cos(\theta_{\mathrm{r}}) - \gamma_{\mathrm{s}}c\beta_{\mathrm{s}}\cos(\theta_{\mathrm{s}})\left[\sin^2(\theta_{\mathrm{r}}) + \gamma_{\mathrm{r}}\cos^2(\theta_{\mathrm{r}})\right] \\ &\quad \mp\gamma_{\mathrm{s}}(\gamma_{\mathrm{r}}-1)c\beta_{\mathrm{s}}\frac{\sin(\theta_{\mathrm{s}})\sin(2\theta_{\mathrm{r}})}{2} \\ N_\mp &= \gamma_{\mathrm{s}}\gamma_{\mathrm{r}}[1 \mp \beta_{\mathrm{s}}\beta_{\mathrm{r}}\cos(\theta_{\mathrm{s}})\cos(\theta_{\mathrm{r}}) - \beta_{\mathrm{s}}\beta_{\mathrm{r}}\sin(\theta_{\mathrm{s}})\sin(\theta_{\mathrm{r}})] \end{aligned}\right. \tag{20}$$

with the involved parameters given by

The reflection/transmission coefficients $\tilde{R}^{\mathrm{TE}}$ and $\tilde{T}^{\mathrm{TE}}$ defined in this frame, which are functions of $\tilde{\omega}, \tilde{k}_x$ (frequency and wavevector defined in $\tilde{S}$ frame), are obtained by substituting

$$\begin{aligned} \omega &= \gamma_{\mathrm{r}}(\tilde{\omega} + \cos\theta_{\mathrm{r}} v_{\mathrm{r}} \tilde{k}_x + \sin\theta_{\mathrm{r}} v_{\mathrm{r}} \tilde{k}_z) \\ k_x &= [1 + (\gamma_{\mathrm{r}} - 1)\cos^2\theta_{\mathrm{r}}]\tilde{k}_x + (\gamma_{\mathrm{r}} - 1)\cos\theta_{\mathrm{r}}\sin\theta_{\mathrm{r}}\tilde{k}_z \\ &\quad + \gamma_{\mathrm{r}}\cos\theta_{\mathrm{r}}\beta_{\mathrm{r}}\frac{\tilde{\omega}}{c} \end{aligned} \tag{21}$$

with $\tilde{\Delta} = \tilde{k}_{1z}/(\tilde{k}_{0z}\tilde{\mu}_{\mathrm{r}})$ and

$$\tilde{k}_{1z} = \sqrt{\tilde{\varepsilon}_{\mathrm{r}}\tilde{\mu}_{\mathrm{r}} \cdot \left[\gamma_{\mathrm{r}}\left(\frac{\tilde{\omega}}{c} + \beta_{\mathrm{r}}\tilde{k}_x\right)\right]^2 - \left[\gamma_{\mathrm{r}}\left(\tilde{k}_x + \frac{\beta_{\mathrm{r}}\tilde{\omega}}{c}\right)\right]^2}. \tag{22}$$

into Eq. (15). It is interesting to note that the *effective* permittivity $\tilde{\varepsilon}_{\mathrm{r}}$ and permeability $\tilde{\mu}_{\mathrm{r}}$ of the metamaterial seen at this frame should be

$$\begin{aligned} \tilde{\varepsilon}_{\mathrm{r}}(\tilde{\omega}, \tilde{k}_x) &= \varepsilon_{\mathrm{r}}(\gamma_{\mathrm{r}}\tilde{\omega} + \gamma_{\mathrm{r}} v_{\mathrm{r}}\tilde{k}_x), \\ \tilde{\mu}_{\mathrm{r}}(\tilde{\omega}, \tilde{k}_x) &= \mu_{\mathrm{r}}(\gamma_{\mathrm{r}}\tilde{\omega} + \gamma_{\mathrm{r}} v_{\mathrm{r}}\tilde{k}_x), \end{aligned} \tag{23}$$

which are dependent on $\tilde{k}_x$. Eq. (23) shows that the system becomes *spatially dispersive* seen in the $\tilde{S}$ frame. This is a typical consequence of a moving medium since the metamaterial slab is now moving when seen in this frame [21].

In some situations, we need the Fourier component form of the field. In the ideal case, applying a standard Fourier transform over the time interval $[-\infty,\infty]$, $\tilde{E}_y(\tilde{\vec{r}}, \tilde{\omega}) = \int_{-\infty}^{\infty} \tilde{E}_y(\tilde{\vec{r}}, \tilde{t}) e^{i\tilde{\omega}\tilde{t}} d\tilde{t}$, we find that the Fourier component of $\tilde{E}_y$ field in region 0 is

$$\begin{aligned} \tilde{E}_y(\tilde{\vec{r}}, \tilde{\omega}) &= \frac{i\mu_0 I_0}{4\pi}\int d\tilde{k}_x e^{i\tilde{k}_x\tilde{x}} \\ &\quad \left[\Omega_-(\tilde{\omega}, \tilde{k}_x) e^{-i\tilde{k}_{0z}\tilde{z}} + \Omega_+(\tilde{\omega}, \tilde{k}_x)\tilde{R}^{\mathrm{TE}} e^{i\tilde{k}_{0z}\tilde{z}}\right]. \end{aligned} \tag{24}$$

Other field components can be derived similarly.

3. Benchmark results

As a benchmark test, we now employ our theory to study the Doppler effects in vacuum (i.e., assuming that there is no metamaterial slab). Apparently, we have $\tilde{R}^{\mathrm{TE}} \equiv 0$ in such a case. Since now both the source and the receiver are moving, the frequency of the signal received by the moving receiver could be different from the source frequency ω_0. This is known as the Doppler effect.

We first consider an exact solvable case in which both the source and receiver are moving on the same line along the x direction. Ideally, the Doppler signal frequency is determined by the peak position of the spectrum function $\tilde{E}_y(\tilde{\vec{r}}, \tilde{\omega})$ of the received EM wave. Assuming that the receiver is located at $\tilde{x} = d, \tilde{z} = 0$ in the $\tilde{S}$ frame, we found that the spectrum function of the signal received by the receiver is given by

$$\tilde{E}_y(\tilde{\vec{r}}, \tilde{\omega}) = \frac{i\mu_0 I_0}{4\pi}\int d\tilde{k}_x e^{i\tilde{k}_x d}\Omega_-(\tilde{\omega}, \tilde{k}_x). \tag{25}$$

We note from Eq. (19) that the function $\Omega_-(\tilde{\omega}, \tilde{k}_x)$ contains two terms. Considering that there is an integration over $\tilde{k}_x$ in Eq. (25), we understand that both terms in $\Omega_-(\tilde{\omega}, \tilde{k}_x)$ in Eq. (19) must diverge simultaneously to make $\tilde{E}_y(\tilde{\vec{r}}, \tilde{\omega})$ exhibit a peak. This results in the following conditions,

$$\begin{aligned} &C_-\tilde{k}_{0z} + D_-\tilde{k}_x + \frac{E_-\tilde{\omega}}{c} = 0 \\ &L_-\tilde{k}_{0z} + M_-\tilde{k}_x + N_-\tilde{\omega} - \omega_0 = 0 \end{aligned} \tag{26}$$

Noting that the source/receiver are both moving along the x direction, we found from Eq. (20) that the involved parameters are

$$\begin{aligned} &C_- = 1, \quad D_- = 0, \quad E_- = 0 \\ &L_- = 0, \quad M_- = \gamma_{\mathrm{s}}\gamma_{\mathrm{r}}[c\beta_{\mathrm{r}} - c\beta_{\mathrm{s}}], \quad N_- = \gamma_{\mathrm{s}}\gamma_{\mathrm{r}}[1 - \beta_{\mathrm{s}}\beta_{\mathrm{r}}]\,, \end{aligned} \tag{27}$$

Thus, Eq. (26) becomes

$$\tilde{k}_{0z} = 0 \tag{28a}$$

$$\gamma_{\mathrm{s}}\gamma_{\mathrm{r}}[c\beta_{\mathrm{r}} - c\beta_{\mathrm{s}}]\tilde{k}_x + \gamma_{\mathrm{s}}\gamma_{\mathrm{r}}[1 - \beta_{\mathrm{s}}\beta_{\mathrm{r}}]\tilde{\omega} - \omega_0 = 0. \tag{28b}$$

Simple calculation shows that the solution of (28) is given by

$$\tilde{\omega} = \frac{\omega_0}{\gamma_{\mathrm{s}}\gamma_{\mathrm{r}}[1 - \beta_{\mathrm{s}}\beta_{\mathrm{r}}] + \gamma_{\mathrm{s}}\gamma_{\mathrm{r}}[\beta_{\mathrm{r}} - \beta_{\mathrm{s}}]}, \tag{29}$$

which is the Doppler signal frequency. Let us consider several limiting cases of Eq. (29). When only the source is moving (i.e., $\beta_{\mathrm{r}} = 0$, $\gamma_{\mathrm{r}} = 1$), we get

$$\tilde{\omega} = \omega_0\sqrt{\frac{1 + \beta_{\mathrm{s}}}{1 - \beta_{\mathrm{s}}}}. \tag{30}$$

Meanwhile, when only the receiver is moving (i.e., $\beta_{\mathrm{s}} = 0$, $\gamma_{\mathrm{s}} = 1$), we get

$$\tilde{\omega} = \omega_0\sqrt{\frac{1 - \beta_{\mathrm{r}}}{1 + \beta_{\mathrm{r}}}}, \tag{31}$$

One immediately finds that Eqs. (31) and (30) are identical if we interchange β_{r} and $-\beta_{\mathrm{s}}$, which is the expected result. Finally, if the source and the receiver

have the same velocities, we found that

$$\tilde{\omega} = \omega_0. \tag{32}$$

indicating that there is no Doppler shift in this case. Eqs. (30)–(32) are consistent with the standard Doppler effects described in textbook [20,21], serving as the benchmark tests to validate our theory.

Our theory can also be applied to the more general situations where $\vec{v}_s$, $\vec{v}_r$ are arbitrary and the source and receiver are not moving on the same line. In those cases, analytical solutions are difficult to obtain, since the integrations over $\tilde{t}$ should *not* be done over the $[-\infty,\infty]$ interval as we did in Eq. (24) to get the Fourier component of the received signal. In fact, in such cases, the Doppler frequency strongly depends on the exact time when we measure the signal. Therefore, we performed the time integrations over a time interval $[\tilde{t}_0 - \delta\tilde{t}/2, \quad \tilde{t}_0 + \delta\tilde{t}/2]$ around each time instance $\tilde{t}_0$ that we measure the signal. The time interval $\delta\tilde{t}$ is chosen large enough to cover several tens of time periods, while small enough inside which the relative configuration between source and receiver does not change significantly. Here we consider the configuration as shown in the inset to Fig. 2(a) and take $\delta\tilde{t} = 60\,2\pi/\omega_0$ to calculate the Doppler frequencies at different measuring time $\tilde{t}_0$. We assume that the source is moving at a velocity $v_s = 0.01c$, and the receiver is at rest and located at $\tilde{x} = 60\lambda_0$, $\tilde{z} = -0.6\lambda_0$ in the $\tilde{S}$ frame, where λ_0 is the wavelength measured in the S frame.

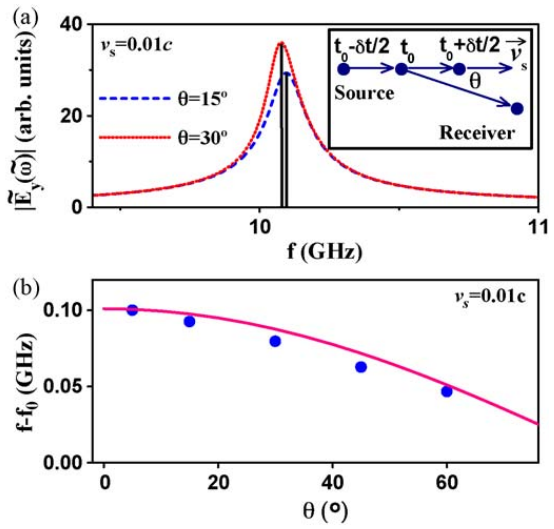

Fig. 2. (a) E-field frequency spectrum measured by the receiver at two different time instances determined by θ. Inset shows the geometry and the calculation strategy. (b) Doppler frequency shift as a function of measuring time specified by θ, obtained by our full-wave dynamical theory (solid circles) and the standard formula $f = \gamma f_0\ (1 + \beta\cos(\theta))$ with $f_0 = 10$ GHz (line).

Therefore, at different time instance $\tilde{t}_0$, the line connecting the source and receiver exhibits a different angle θ with respect to the x axis, so that $\tilde{t}_0$ has a one-by-one correspondence with θ, as shown in the inset to Fig. 2(a). Fig. 2(a) shows the field spectra measured at two different time instances specified by different values of θ. We can clearly find that there is a well-defined Doppler frequency in each spectrum, but the two Doppler frequencies are different. Fig. 2(b) depicts the Doppler frequency shift for 5 different values of θ. Obviously, the frequency shift $\Delta f (f = \omega/2\pi$ is the linear frequency) is a decreasing function of θ before reaching a minimum at $\theta = \pi/2$. Despite of some small discrepancies, the Doppler shift calculated by our full-wave dynamical theory is in quantitative agreement with the relativistic Doppler shift formula $f = \gamma f_0(1 + \beta\cos(\theta))$ (solid line) recorded in textbook [20], which was usually obtained under the ray approximation.

4. Applications of the theory

Obviously, the established theory is very suitable to study the optical phenomena related to the moving source/receiver/environment. For example, when both the source and the receiver are placed on top of a metamaterial slab, the Doppler effects would be very intriguing. In our previous work [23], we have considered a special case in which the source is static while the receiver is moving with respect to the slab, but the general cases in which both the source and receiver are moving would be more interesting. On the other hand, many fascinating optical phenomena (such as the super imaging and the invisibility cloaking) demonstrated so far were typically studied and/or observed in a static situation [24–26]. It is natural to ask what happens if the source, receiver and the lens are in relative motions.

In this section, we present two examples to illustrate the applications of our theory. We first consider the anomalous Doppler effects in a more complicated situation, i.e., both source and receiver are moving along the x direction at different velocities. We next study the influences of the relative motions on the super lensing effect [6,7]. Without losing generality and for definiteness, in all our numerical calculations, we assume that the metamaterial slabs studied in both cases possess a Drude-like permittivity and permeability function $\varepsilon_r(f) = \mu_r(f) = 1\text{–}200/f(f + i\delta)$ with $\delta = 10^{-4}/2\pi$ GHz, where f is the linear frequency measured in GHz. However, we emphasize that the phenomena reported here are independent of the concrete forms of $\varepsilon_r(\omega)$, $\mu_r(\omega)$ that we adopted.

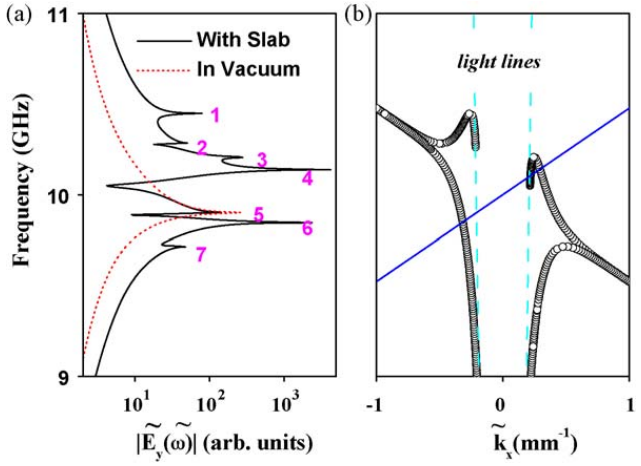

Fig. 3. (a) E-field frequency spectra measured by the receiver when the source and receiver are moving at velocities $v_s = 0.02c$, $v_r = 0.01c$ near the metamaterial slab (solid line) and in the vacuum (dotted line). (b) The surface wave dispersion diagram of the metamaterial seen at the $\tilde{S}$ frame (circles), the light lines (dashed lines) and the solution of Eq. (28b) (solid line).

4.1. The Doppler effects

We first employ our theory to study the anomalous Doppler effects. We assume the receiver is placed at $\tilde{x} = 0, \tilde{z} = -0.499d$ in its own frame (very near the metamaterial slab). Seen at the S frame, the source and receiver are moving along the x direction at velocities $v_s = 0.02c\vec{e}_x$ and $v_r = 0.01c\vec{e}_x$ with respect to the metamaterial slab**.** The working frequency of the source is $f_0 = 10$ GHz. Employing our theory, we calculated the spectrum function $\tilde{E}_y(\tilde{\omega})$ for the field received by the receiver and depicted the spectrum in Fig. 3 (a) as a solid line. While the geometry is almost the same as the benchmark test that we presented in the last section, surprisingly, here we found that the received signal possesses seven prominent peaks [see Fig. 3(a)]. Removing the metamaterial slab, we re-calculated the spectrum and depicted it as a dotted line in the same figure. The comparison shows that, among the 7 peaks depicted in Fig. 3(a), only 1 (peak no. 5) corresponds to the normal Doppler shift mode observed also in vacuum. The other 6 modes must be contributed by the metamaterial slab since they disappear when the metamaterial slab is absent.

To explore the physics behind such unusual phenomena, we depicted in Fig. 3(b) the surface wave (SW) dispersions of the metamaterial slab (seen at the receiver-static frame $\tilde{S}$), which are defined as the poles of the reflection spectra $\tilde{R}^{\mathrm{TE}}(\tilde{\omega}, \tilde{k}_x)$ measured in the $\tilde{S}$ frame. The SW dispersion of a metamaterial slab has been extensively studied in literature [27–29]. However, since the slab is moving in the $\tilde{S}$ frame, the SW dispersion diagram is quite unusual, as shown in Fig. 3(b). Compared with the conventional dispersion diagram, we found that the dispersion diagram for a moving metamaterial is distorted, and becomes asymmetrical for $\pm\tilde{k}_x$. This can be explained by the fact that the $\tilde{\varepsilon}_r, \tilde{\mu}_r$ functions are $\tilde{k}_x$ dependent in the $\tilde{S}$ frame since the metamaterial slab is moving [see Eq. (23)].

On the other hand, since the source is also moving with respect to the metamaterial slab, the source spectrum, characterized by the function $\Omega_{\mp}(\tilde{\omega}, \tilde{k}_x)$, also changes significantly. It has been argued (in Section 3) that the Doppler signal frequency is determined by the condition that the integrand in Eq. (24) has two terms diverting simultaneously. The divergence in $\tilde{R}^{\mathrm{TE}}(\tilde{\omega}, \tilde{k}_x)$ has been known as the SW spectrum, already plotted as open circles in Fig. 3(b). Meanwhile, the divergence in the function $\Omega_{\mp}(\tilde{\omega}, \tilde{k}_x)$ is determined by two separate Eqs. (28a) and (28b). We have plotted the solutions of (28a) as two dashed lines in Fig. 3(b) and the solutions of (28b) as a solid line in Fig. 3(b). Interestingly, we find that the two dashed lines are just the light lines that satisfy $\tilde{\omega} = \pm c\tilde{k}_x$.

These three types of lines can help us identify the origins of those additional Doppler modes easily. For example, we immediately found that peaks' nos. 1, 2, 3 and 7 coincide with those frequencies at which the density of states (DOS) for the SW (proportional to $\partial\tilde{\omega}/\partial\tilde{k}_x = 0$) are divergent. These high-DOS states are excited by the transient components of the source, and then generate additional peaks in the received field spectrum, as also observed in our previous work [23]. Mathematically, at these high-DOS SW states, reflection function $\tilde{R}^{\mathrm{TE}}$ exhibits a second-rank divergent pole so that an integration over $\tilde{k}_x$ can not overcome its divergence, and therefore, a peak is left in the spectrum $\tilde{E}(\tilde{\omega})$. On the other hand, peaks' nos. 4 and 6 are of different origins, and have not been observed in previous studies [23]. A direct inspection reveals that these two peaks appear at the intersection points between the source spectrum [(blue) solid line, Eq. (28b)] and the SW dispersion curve (open circles). However, one must be careful since *not* all of these intersection points contribute to the spectrum peaks. For example, the intersection point lying in-between the peaks' nos. 4 and 5 does not contribute a spectrum peak. The reason accounting for such unusual behaviors is the causality requirement. Recalling that $v_s > v_r$ along the x direction, which means that the source is always at $+\tilde{x}$ direction with respect to the receiver in the $\tilde{S}$ frame, it is easy to understand that only those SW's with group velocities along $-\tilde{x}$ direction can be caught by the

receiver. Since at peaks' nos. 4 and 6, the SW dispersions exhibit negative group velocities, the SWs excited by the source will travel along $-\tilde{x}$ direction so that they can be grasped by the receiver as strong Doppler signals. Meanwhile, at the other intersection point, the SW exhibits a positive group velocity, so that this SW (even it can be excited) cannot be grasped by the receiver as a Doppler signal.

4.2. Super lensing of a moving source

We understand that a left-handed metamaterial slab with $\varepsilon = \mu = -1$ has been used to focus the EM waves to break the usual diffraction limit [5]. However, the studies performed so far were all based on the assumption that the source and super lens are static [6,7,24,25]. In reality, this is not necessarily always the case. Let us now study the super focusing effect of a metamaterial lens which is moving with respect to the source. Assume that the working frequency is $f_0 = 10$ GHz such that the real parts of $\varepsilon_r(\omega)$, $\mu_r(\omega)$ all nearly equal to -1, we first studied the focusing effect in the case that the slab is static. The calculated field distribution of the image on the image plane at $z = -2d$ (See Fig. 1) is shown as (red) solid circles in Fig. 4, which shows a sharp peak with a subwavelength width. The physics of such super resolution is easily understood from the SW dispersion of the metamaterial slab, which is depicted in Fig. 5 also as (red) solid circles. At the working frequency, the SW mode exhibits a very large k_x value (bounded only by the finite dissipation δ) so that very high spatial oscillations can be collected by the lens, leading to a very high image resolution.

Things completely change when the super lens is moving with respect to the source and the receiver.

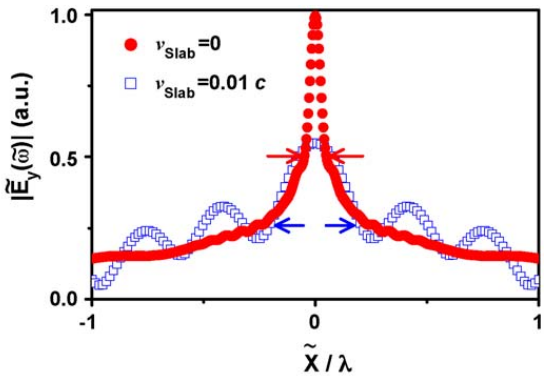

Fig. 4. Electric field distributions measured on the image plane, for the metamaterial lens at rest (solid circles) and moving at a velocity $v_{slab} = 0.01c$ (open squares), with the arrows defining the half-maximum peak widths.

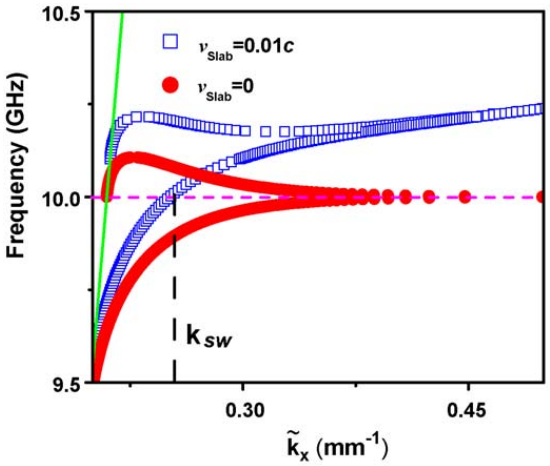

Fig. 5. Surface wave dispersions of the metamaterial lens at rest (solid circles) and moving at a velocity $v_{slab} = 0.01c$ (open squares).

Assuming that the super lens is moving along the x axis at a velocity $0.01c$, we employed our dynamical theory to re-calculate the instantaneous field distribution of the image, and plotted the results as (blue) open squares in Fig. 4. We found that the image peak significantly broadens with some undesirable side loops. These intriguing phenomena can again be understood from the SW dispersion which is recorded in Fig. 5 also as (blue) open squares. Since the slab is moving now, seen at the $\tilde{S}$ frame, the permittivity and permeability function [given by Eq. (23)] change significantly, leading to dramatic modifications of the SW dispersion curve as shown by the (blue) open squares in Fig. 5. Therefore, at the working frequency f_0, the SW mode takes a finite value $k_x = k_{sw}$, which is significantly reduced as compared to that in the static case [30]. As a result, the moving super lens could collect much less evanescent wave components than a static one so that the image resolution deteriorates significantly.

5. Conclusions

In short, we have presented in this paper a general dynamical Green's function approach, which could be employed to study the optical phenomena in a situation where the source, receiver and/or the metamaterial environment are moving with respect to each other. Here, the Lorentz transformations are used to treat the movements of the source and/or the receiver. After presenting some benchmark tests to justify our theory, we employed the dynamical theory to study the anomalous Doppler effects as well as the super lensing effects related to a moving source and/or metamaterial. We believe that the present theory can be applied to study many other intriguing optical phenomena.

Acknowledgements

This work was supported by the China-973 Program (2006CB921701), the NSFC (60725417, 60990321), Shanghai science and technology committee (no. 08dj1400302) and PCSIRT.

References

[1] D.R. Smith, W.J. Padilla, D.C. Vier, S.C. Nemat-Nasser, S. Schultz, Phys. Rev. Lett. 84 (2000) 4184.
[2] R.A. Shelby, D.R. Smith, S. Schultz, Science 292 (2001) 77.
[3] D.R. Smith, J.B. Pendry, M.C.K. Wiltshire, Science 305 (2004) 788.
[4] V.G. Veslago, Sov. Phys. Usp. 10 (1968) 509.
[5] J.B. Pendry, Phys. Rev. Lett. 85 (2000) 3966.
[6] F. Mesa, M.J. Freire, R. Marqués, J.D. Baena, Phys. Rev. B 72 (2005) 235117.
[7] Xiang Zhang, Zhaowei Liu, Nat. Mater. 7 (2008) 435.
[8] A.V. Kats, V.A. Sergey Savel'ev, Yampol' skii, Franco Nori, Phys. Rev. Lett. 98 (2007) 073901.
[9] M. Einat, E. Jerby, Phys. Rev. E 56 (1997) 5996.
[10] E.J. Reed, M. Soljăcic′, J.D. Joannopoulos, Phys. Rev. Lett. 91 (2003) 133901.
[11] N. Seddon, T. Bearpark, Science 302 (2003) 1537.
[12] A.B. Kozyrev, D.W. von der Weide, Phys. Rev. Lett. 94 (2005) 203902.
[13] X.H. Hu, Z.H. Hang, J. Li, J. Zi, C.T. Chan, Phys. Rev. E 73 (2006) 015602.
[14] C.Y. Luo, M. Ibanescu, E.J. Reed, S.G. Johnson, J.D. Joannopoulos, Phys. Rev. Lett. 96 (2006) 043903.
[15] I.V. Shadrivov, A.A. Sukhorukov, Y.S. Kivshar, Phys. Rev. Lett. 95 (2005) 193903.
[16] Shulin Sun, Xueqin Huang, Lei Zhou, Phys. Rev. E 75 (2007) 066602.
[17] U. Lehonhardt, Science 312 (2006) 1777.
[18] J.B. Pendry, D. Schurig, D.R. Smith, Science 312 (2006) 1780.
[19] R.W. Ziolkowski, A.D. Kipple, Phys. Rev. E 68 (2003) 026615.
[20] J.D. Jackson, Classical Electrodynamics, Wiley, New York, 1962.
[21] J.A. Kong, Electromagnetic Wave Theory, Higher Education Press, 2002.
[22] Y. Zhang, T.M. Grzegorzyk, J.A. Kong, Electromagn. Waves 35 (2002).
[23] Weihua Wang, Xueqin Huang, Lei Zhou, C.T. Chan, Opt. Lett. 33 (2008) 369.
[24] Atsushi Ono, Jun-ichi Kato, Satoshi Kawata, Phys. Rev. Lett. 95 (2005) 267407.
[25] Nicholas Fang, Hyesog Lee, Cheng Sun, Xiang Zhang, Science 308 (2005) 534.
[26] I.I. Smolyaninov, V.N. Smolyaninova, A.V. Kildishev, V.M. Shalaev, Phys. Rev. Lett. 102 (2009) 213901.
[27] R. Ruppin, Phys. Lett. A 277 (2003), 61 (2000).
[29] Armando Giannattasio, W.L. Barnes, Opt. Expr. 13 (2005) 428.
[30] D.R. Smith, D. Schurig, M. Rosenbluth, S. Schultz, S.A. Ramakrishna, J.B. Pendry, Appl. Phys. Lett. 82 (2003) 1506.